Reaction Kinetics, Mechanisms and Catalysis (2022) 135:1635–1649
https://doi.org/10.1007/s11144-022-02213-x

Influence of alumina pH on properties of Fe_2O_3/Al_2O_3 catalyst for high-density polyethylene decomposition to H_2 generation

L. A. Flores-Sánchez[1] · J. M. Quintana-Melgoza[1] · M. A. Armenta[2] · O. E. Jaime-Acuña[3] · R. Obeso-Estrella[1] · M. Avalos-Borja[4]

Received: 9 February 2022 / Accepted: 30 March 2022 / Published online: 7 April 2022

Abstract

A synthesis of Fe_2O_3 supported on acid, neutral and basic Al_2O_3 was carried out by an incipient wet impregnation to test the obtained materials on catalytic decomposition of a high-density polyethylene reaction of H_2 production. All materials were characterized by an X-ray diffraction, scanning electron microscopy, energy dispersion spectroscopy, surface area and the H_2 and CH_4 production by gas chromatography. Results show that the crystal size, particle size and surface area decrease as the pH of the supports increases, the morphology, and the dispersion of the nanoparticles of Fe_2O_3. This work demonstrates the ability to produce H_2 from the catalytic decomposition of high-density polyethylene (Fe_2O_3/a-Al_2O_3: 62%) at low temperatures (about 200 °C lower *vs* other reports).

✉ L. A. Flores-Sánchez
lflores94@uabc.edu.mx

[1] Universidad Autónoma de Baja California, Calzada Universidad, 14418, Parque Industrial Internacional Tijuana, Tijuana B.C. C.P. 22390, Mexico

[2] Departamento de Ingeniería en Geociencias, Universidad Estatal de Sonora, Av. Niños Héroes, San Javier, 84160 Magdalena de Kino, Sonora, Mexico

[3] Centro de Nanociencias y Nanotecnología, UNAM, Apartado Postal 14, Ensenada B. C. C.P. 22800, Mexico

[4] División de Materiales Avanzados, Instituto Potosino de Investigación Científica y Tecnológica, Camino a la Presa San José 2055, Lomas 4ta sec., C.P. 78216 San Luis Potosí, S.L.P., Mexico

Graphical abstract

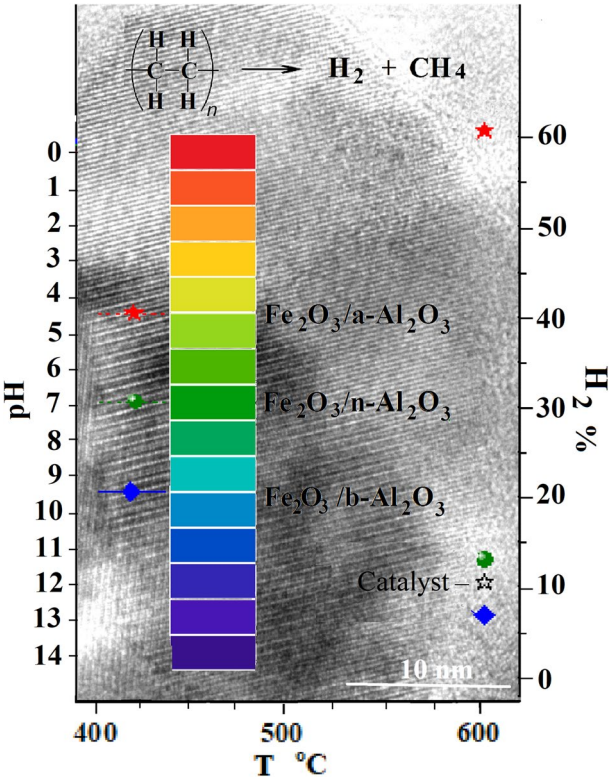

Keywords Fe_2O_3 synthesis · pH Al_2O_3 · Polyethylene · Molecular hydrogen production

Introduction

The production of polyolefins such as high-density polyethylene (HDPE) is of utmost importance despite the fact that current environmental problems and regulations have made producers and consumers aware of the relative responsibility of plastics. However, HDPE is still a global problem since it contributes with 12.2% of the global production of residual plastics and according to the reports it will continue to increase [1]. It was reported in 2020, that approximately 79 Mt (metric ton) of polyethylene were produced globally, of which only 19 Mt are recycled, 43 Mt were disposed of in landfill and 17 Mt were used in energy recovery processes. Currently there is a wide variety of initiatives based on the fluid catalytic cracking (FCC) process, which proposed that oil refineries can be turned into solid plastic waste refineries and thus transform municipal solid waste such as HDPE into

oil derivatives [2, 3], some other proposals have been based on other processes like thermochemical decomposition or pyrolysis [4–8]. For all those reasons, we chose HDPE as a raw material for the catalytic production of clean fuels such as molecular hydrogen [1–10]. Multiple reports have been found from the 70s to the present, where the obtention and mechanisms of the production of hydrocarbons, as well as molecular hydrogen by thermal and catalytic methods from HDPE, continue to be studied [11–13]. Several alumina supported catalysts have been used in the production of H_2 from HDPE, however, the influence of pH supports for these materials has not been explored yet. Fe-based materials supported on Al_2O_3 [14, 15] have been reported in the production of H_2 from the catalytic degradation on solid waste such as HDPE. In this work, the synthesis of materials based on iron oxide supported on acidic (a-Al_2O_3), neutral (n-Al_2O_3) and basic (b-Al_2O_3) alumina, is reported. The main purpose is to know the effect of pH support on the crystalline, morphological, structural, surface and catalytic properties of Fe_2O_3 and its relationship with their capacity to produce H_2 from HDPE by catalytic degradation. For this purpose, the materials were characterized by XRD, SEM, EDS, BET, NH_3–TPD, and tested on catalytic production of molecular hydrogen from HDPE.

Experimental

Synthesis of the ferric oxide (III) (Fe_2O_3) on acidic (a-Al_2O_3), neutral (n-Al_2O_3) and basic (b-Al_2O_3) alumina was carried out by a variation in the incipient wet impregnation methodology. Briefly, $Fe(NO_3)_3{\cdot}9H_2O$ (Aldrich 216828) were homogenously mixed (5% w/w Fe) with the selected support material (95% w/w) (commercial alumina a-Al_2O_3 Aldrich 199966, b-Al_2O_3 Aldrich 199,443 and n-Al_2O_3 Aldrich 19997-4) and placed inside of a porcelain combustion boat to rest during 24 h at room temperature. Then, they were introduced in a Lindberg Blue M high-temperature electric tubular furnace for 1 h at a certain temperature (400, 500, 600 °C) along with an air flow (60 $cm^3\ min^{-1}$). Finally, the system was cooled down to room temperature, afterwards the samples were recovered. Table 1 summarizes the synthesis conditions for each sample. In order to identify the crystalline phases, a XRD analysis was performed on a BRUKER D8 ADVANCE XRD using Cu K_α radiation (40 kV, 30 mA). Data from JCPDS-ICCD database [16] were used to identify all the phases. Crystal size (CZ) was calculated through the Scherrer equation (Eq. 1), [17] using as main peaks those attributed to plane (104) for Fe_2O_3 and (440) for γ-Al_2O_3.

Table 1 Sample summary, Fe_2O_3 supported in Al_2O_3 at 600 °C (1 h at 60 $cm^3\ min^{-1}$ ultra-dry air flow)

Material	Name	Precursor characteristics Al_2O_3	Oxide Precursor
Fe_2O_3/a-Al_2O_3	FeA	pH: 4.5 (in H_2O), 58 Å pore size	$Fe(NO_3)_3{\cdot}H_2O$
Fe_2O_3/n-Al_2O_3	FeN	Standard grade, 58 Å pore size	$Fe(NO_3)_3{\cdot}H_2O$
Fe_2O_3/b-Al_2O_3	FeB	pH: 9.5 (in H_2O), 58 Å pore size	$Fe(NO_3)_3{\cdot}H_2O$

Where: K is a dimensionless shape factor, its typical use 0.9, B is the line broadening at half the maximum intensity.

$$CZ = K\lambda/(B\cos\theta_B) \quad (1)$$

SEM–EDS was used to determine the morphology and the elemental composition of both materials were performed on an ESEM FEI QUANTA 200 (20–25) kV scanning electron microscope using carbon tape to fix the sample. Average particle size (PS), standard deviation (σ) and particle size were made from the direct measurement of approximately 100 particles.

For all impregnated materials acidity properties were measured by ammonia desorption experiments (TPD-NH_3) from 100 to 600 °C using a Micromeritics TPR/TPD 2900 instrument provided with a TCD and interfaced to a data station. Supported materials (50 mg) were dried in helium flow at 300 °C for 0.5 h. After samples were cooled to 100 °C, and the inlet gas (100 cm^3 min^{-1}) of ammonia (5% ammonia in He balance) was put in contact with samples for 1 h to ammonia saturation occurred. Next, a 15 min equilibration in helium was performed at the same temperature (100 °C). Finally, a linear heating rate of 10 °C min^{-1} to 600 °C was used for the ammonia desorption analysis. For quantitative analysis, areas of deconvoluted Gaussian curves were integrated and the strength of acid sites were classified as follow; weak acidity from 100 to 300 °C; medium acidity from 300 to 450 °C and; strong acidity around 550 °C.

To determine the catalytic activity of the materials in the decomposition of HDPE to H_2, the following procedure was carried out: 1 g of commercial HDPE that had been previously washed and dried for 0.5 h at 100 °C was placed inside a test tube 24/40 with a 20% w/w catalyst ratio. Subsequently, the tube was mounted in a simple reflux system cooled by air (Fig. 1), a He flow (20 cm^3 min^{-1}) was introduced to the test tube and mediated by a previous vacuum process to eliminate O_2 and N_2 within the system. At the end of the system, a bag (Tedlar Bag SKU: 24655) was connected to collect the reaction gases. After 15, 30, 45 and 60 min of reaction, a sample of 1 cm^3 was taken and injected into a gas chromatograph (GC) (SRI 8610C Gas Chromatograph in which the Alltech Washed Molesieve 5A 80/100 6′ × 1/8″ × 0.085″ SS column). GC analysis conditions were: He flow 25 cm^3 min^{-1}, oven temperature and injector 50 °C, detector 120 °C. The gas chromatograph was standardized using a commercial standard Scott Mini-Mix (1% mol of CO_2, CO, H_2, CH_4 and O_2 diluted on 95 mol% of N_2). For calculations, reference areas of H_2 (0.3365) and CH_4 (14.4965) were obtained by introducing 1 cm^3 of the standard in the GC, this amount corresponds to 6.95×10^{-6} mol. Afterwards, the areas under the curve of the experimental chromatograms (E.A.) were used to obtain the generated amount of substance of H_2 and CH_4 for each 1 cm^3 by using the Eqs. 2 and 3, after this, these experimental calculated amount of substance values were multiplied by the total volume of the obtained gases. Finally, to present the work's results the percentages of hydrogen and methane were calculated (Eqs. 4 and 5) based on the maximum amount of substance expected for each one of them from the maximum

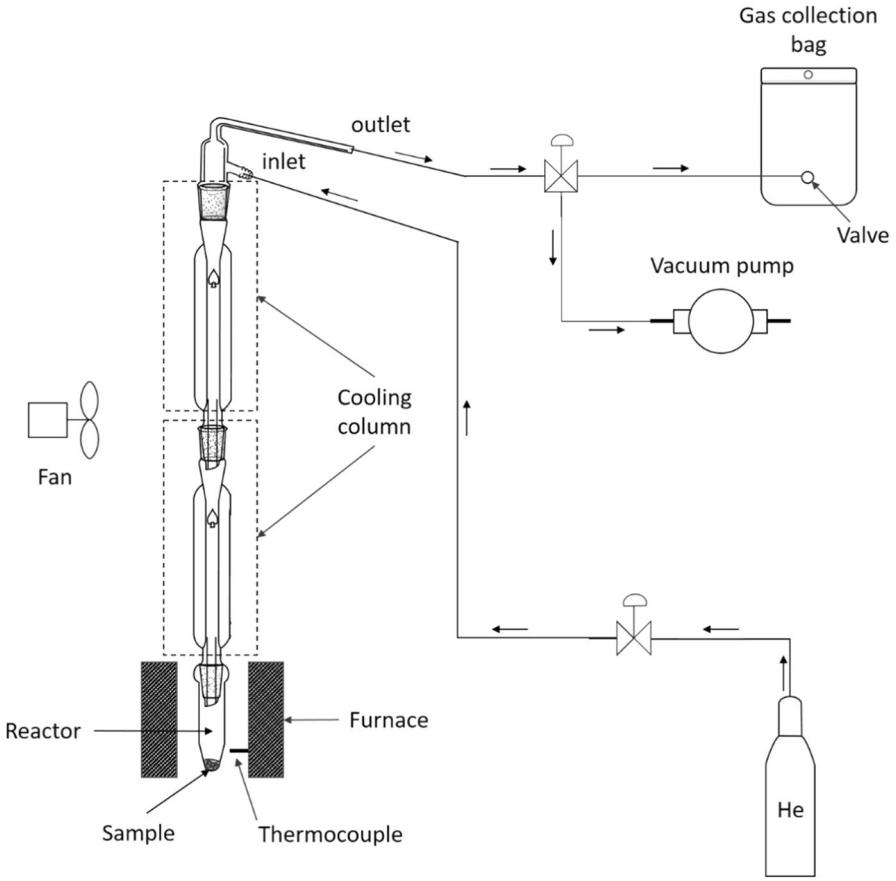

Fig. 1 System diagram for the catalytic production of H_2 from HDPE

content of H (14.21% = 0.0768 mol H_2) and C (85.79% = 0.0384 mol CH_4) by 1 g of HDPE approximately according to some reports [14, 15].

$$\text{mol } H_2 \text{ exp} = \frac{(\text{E.A.})\left(6.9510^{-6} \text{ mol}\right)}{(0.3365)} \tag{2}$$

$$\text{mol } CH_4 \text{ exp} = \frac{(\text{E.A.})\left(6.95\text{x}10^{-6} \text{ mol}\right)}{(14.4965)} \tag{3}$$

$$\%\ H_2 = \frac{\text{experimental mol of } H_2}{0.0768 \text{ mol } H_2} \times 100\% \tag{4}$$

$$\% \, CH_4 = \frac{\text{experimental mol of } CH_4}{0.0384 \text{ mol } CH_4} \times 100\% \quad (5)$$

Results and discussion

Fig. 2 shows XRD from all the impregnated obtained samples at 600 °C, as well as the reported diffractograms cards [16] for Fe_2O_3 and Al_2O_3 corresponding to cards 04-015-9569 and 10-0425, respectively. In addition, the presence of a characteristic γ-Al_2O_3 phase peaks was observed at $2\theta = 66.89°$, 45.85°, 37.80° which correspond to the planes (400), (440), (311). A signal at 42.93° that corresponds to the χ-Al_2O_3 phase was also observable [18]. For iron oxide-based materials, the main signals of ferric oxide (Fe_2O_3) corresponding to planes (104), (110), (012), (024) and (116) were identified in all samples, some signals overlap with the Al_2O_3 phase, however, it was possible to identify the experimental pattern, which confirmed the presence of the Fe_2O_3 phase. Also, the findings showed that the support pH have a significant influence on the crystal size of the Fe_2O_3 (Table 2), where the crystal size decreases as the pH of the supports increase. This observation is in good agreement with that

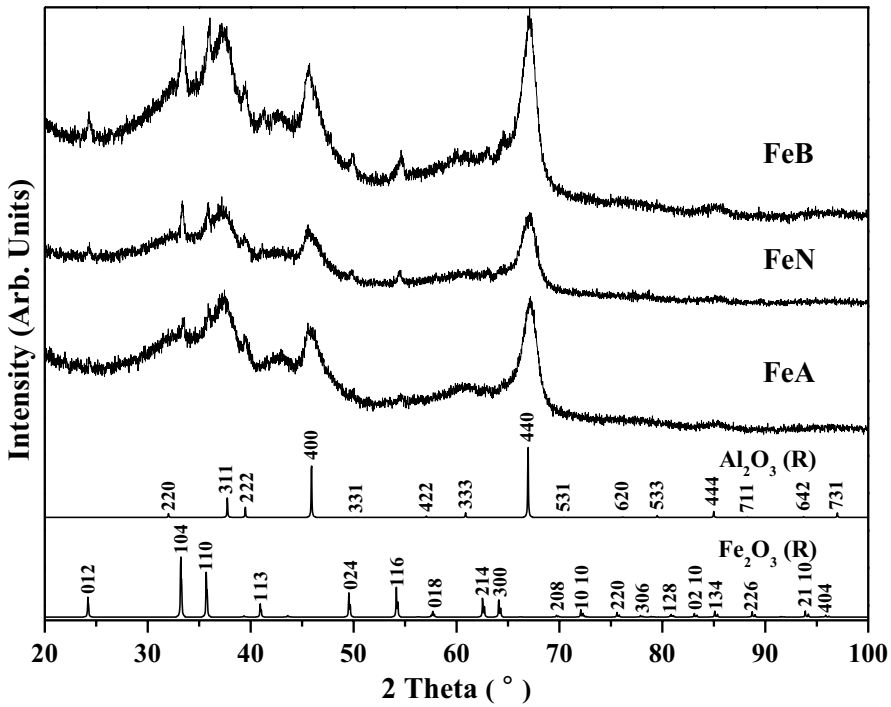

Fig. 2 XRD spectra of phases Fe_2O_3 (Fe) supported over acidic (A), neutral (N) and basic (B) alumina, and reported (R) in data base JCPDS–ICDD

Table 2 Physical properties of catalysts Fe_2O_3 (Fe) supported on acidic (A), neutral (N) and basic (B) alumina synthesized in this work

Catalyst	PS $l \times w \pm \sigma$ (nm)	CS (hkl) (nm)	SA_{BET} ($m^2\ g^{-1}$)	SA_{Lang} ($m^2\ g^{-1}$)	PD (Å)	VP ($cm^3\ g^{-1}$)
A	–	11 (440)	133	183	49.78	0.2407
FeA	$107 \pm 36 \times 56 \pm 11$	30 (104)	109	188	60.83	0.2374
N	–	10 (440)	160	221	43.14	0.2387
FeN	$45 \pm 17 \times 30 \pm 12$	28 (104)	121	209	54.59	0.2309
B	–	12 (440)	127	174	52.28	0.2395
FeB	$34 \pm 14 \times 25 \pm 9$	16 (104)	76	131	65.27	0.1735

Average particle size (PS), length (l), width (w), standard deviation (σ), crystal size (CS): Crystal size calculate using the Scherrer Ec. 1, surface area (SA), pore diameter (PD), volume of pores (VP)

published by H. Kodama et al., [19] where it mentioned that the increase in pH inhibits the crystallization and precipitation. Weak intensities of the Fe_2O_3 signals are due to the small supported concentration (5% w/w). All of this demonstrates that the pH of the support plays an important role in the selection of the final crystal size of the supported phases.

Surface area (BET and Langmuir), pore diameter and pore volume results were presented in Table 2 for all samples (alumina and Fe_2O_3/alumina). All surface areas of the supports decrease after the impregnation process of the oxide phases. FB shows the greatest surface area loss, this is related to the pH of the support, since the basic pH of the alumina causes Fe_2O_3 to form smaller particles, which can be incorporated into the pores of the material not only by surface clogging them, this from the decrease in volume of pores from 0.2395 to 0.1735 $cm^3\ g^{-1}$ (Table 2). It is important to note that the phenomena described on the FB sample can be observed into all the other samples and only the one with the greatest changes has been discussed.

Fig. 3 shows the SEM micrographs, the pH generates observable modifications in the average particle size and dispersion of the Fe_2O_3. The materials show a decrease in the average particle size FA > FN > FB with respect to the increase in the pH of the Al_2O_3. In the dispersion of Fe_2O_3 crystals, the following ranking by pH was found FA < FN < FB. Moreover, an unexpected behavior on the FA sample was observed, and an increase in SA_{Lang} from 183 to 188 $m^2\ g^{-1}$ with respect to a-Al_2O_3 without oxide. Thus, SA_{Lang} is closely related with the external surface of materials, this increase can be explained as a result of the Fe_2O_3 particles that are too large to settle within the pores of the support and preferably the particles are fixed on the external surface. These results allow us to explain those observations and discussions made from XRD and BET experiments.

Fig. 4 shows the EDS spectra of all samples. Supported materials results show the same characteristic signals which correspond to the following energies: 0.70, 0.71, 6.39, 6.40 and 7.05 keV (Fe); 1.48, 1.55 keV (Al) and for 0.52 keV (O). No other external elements were found in any sample, such as contamination or reaction

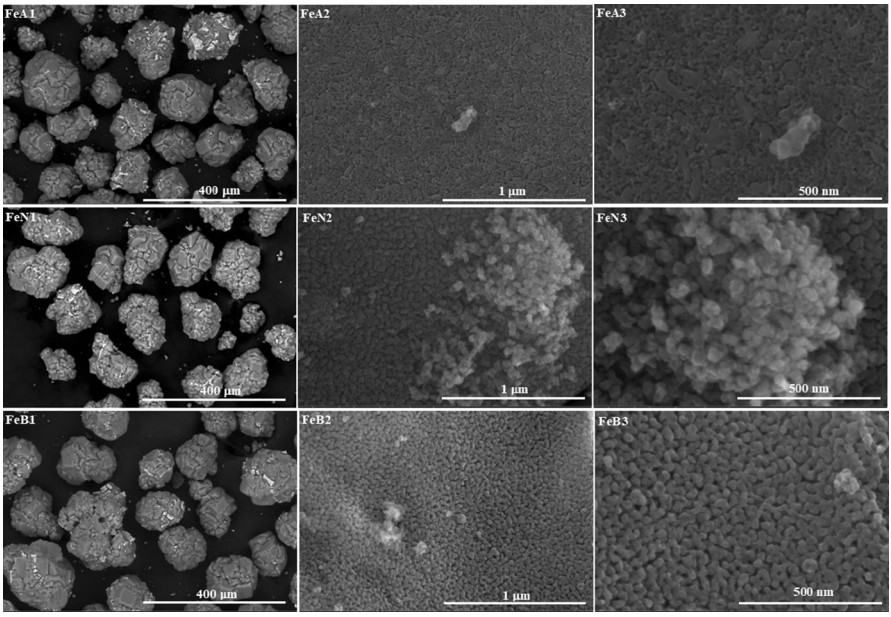

Fig. 3 Micrographs by SEM (SE) of the Fe_2O_3 phase supported on acidic (FeA), neutral (FeN) and basic alumine (FeB), where it is observed that the increase pH generates an effect on the dispersion (FeA3, FeN3 y FeB3) of the Fe_2O_3 phase, as well as a modification in the morphology and particle size

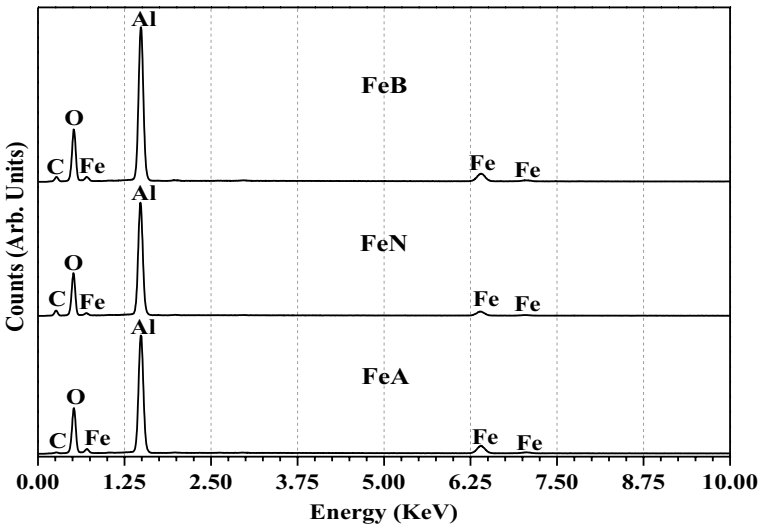

Fig. 4 EDS of oxides Fe_2O_3 supported on acid, neutral and basic alumina

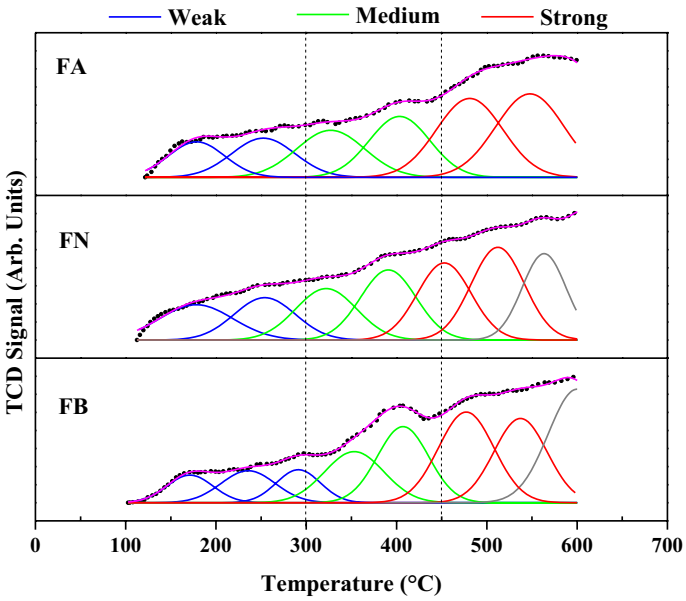

Fig. 5 Comparison of NH_3–TPD profiles of the materials Fe_2O_3/a-Al_2O_3, Fe_2O_3/n-Al_2O_3 and Fe_2O_3/b-Al_2O_3

remnants, which confirms that the proposed methodology is simple, fast and allows to generate the expected phases according to the results obtained by XRD and EDS.

For TPD profiles (Fig. 5) showed a minor TCD signal to FB at low temperature range (100 °C to 300 °C) and there was a marked increase of the signal at medium temperature range (300 °C to 450 °C) in relation to rest of temperature (> 300 °C). Furthermore, FA material showed more intensity in signal at higher temperatures (> 450 °C) respect to at lower temperatures. From quantitative analysis of TPD profiles presented noted fewer differences about sites per gram between FN and FB than respect to FA material. Meanwhile weak and strong acidity difference was notable in FA respect to other catalysts. However, regarding sites density per unit area, the differences were accentuated such as strong acidity sites per unit area increased as follows; FA > FN > FB, whereas for weak and medium acidity these tendencies were modified keeping FN > FB > FA for both.

The production of H_2 and CH_4 after the catalytic decomposition of high-density polyethylene (HDPE) at (400, 500, 600 °C) using Fe_2O_3/a-Al_2O_3 (FA), Fe_2O_3/n-Al_2O_3 (FN), Fe_2O_3/b-Al_2O_3 (FB) as catalysts is shown in Fig. 6. It is important to highlight that the sample Fe_2O_3/a-Al_2O_3 did not present waxes or liquids as by-products after the process at 600 °C, for the rest of the materials and reaction conditions waxes, liquids and/or carbonaceous solids were obtained as by-products. Results in Fig. 6 depict that the H_2 production of all the materials is greater than that shown by thermal decomposition (reaction without catalyst), for this reaction case without catalyst, it is observable that the CH_4 production is greater (43%) in comparison even with the best catalyst sample (16%), the methane production is

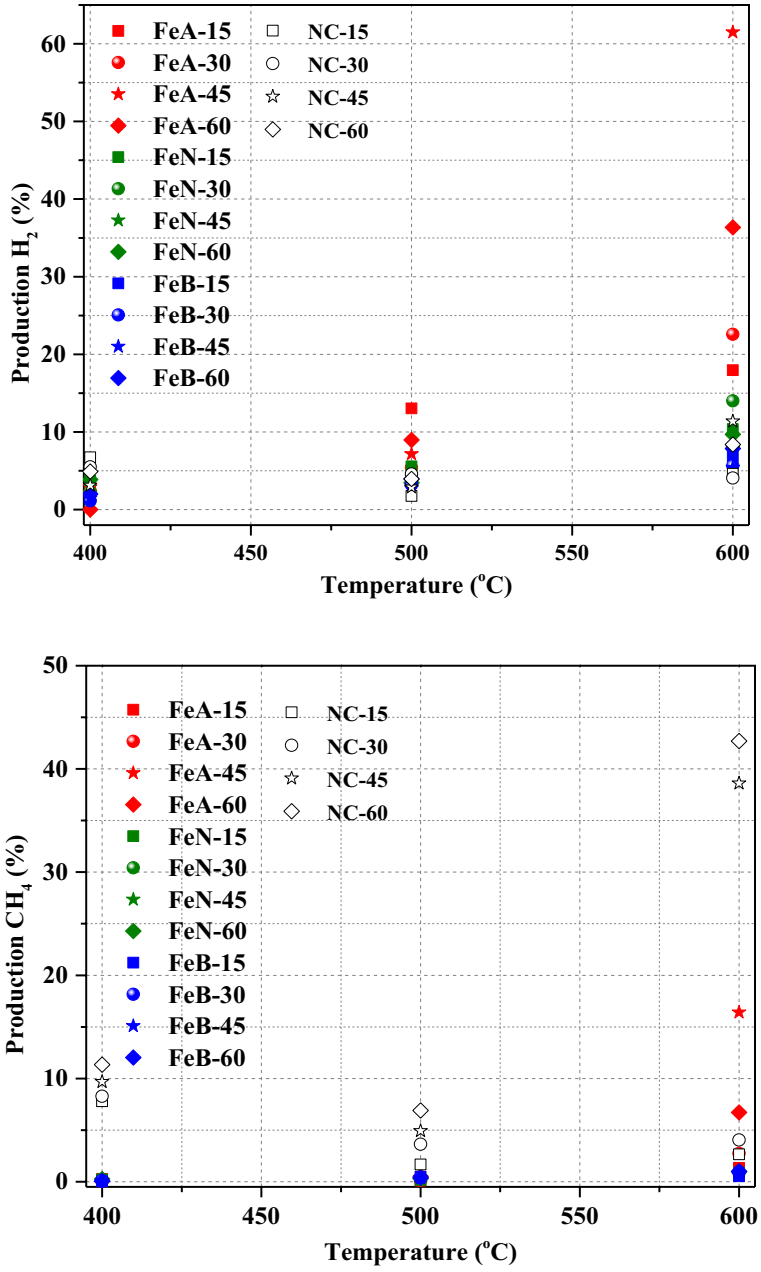

Fig. 6 Production of H_2 and CH_4 from the catalytic decomposition of HDPE at 15 (Square), 30 (Sphere), 45 (Star) and 60 (Diamond) minutes of reaction, with respect to the increase in temperature from 400 to 600 °C (Red: FeA (a-Al_2O_3/Fe_2O_3), green: FeN (n-Al_2O_3/Fe_2O_3), blue: FeB (b-Al_2O_3/Fe_2O_3), black: NC (No catalyst). (Color figure online)

Table 3 NH_3–TPD analysis of samples Fe_2O_3/a-Al_2O_3, Fe_2O_3/n-Al_2O_3 and Fe_2O_3/b-Al_2O_3

Material	Weak acidity		Medium acidity		Strong acidity		Total acidity	
	μmol g^{-1}	mmol m^{-2}	μmol g^{-1}	mmol m^{-2}	μmol g^{-1}	mmol m^{-2}	μmol g^{-1}	mmol m^{-2}
Fe_2O_3/a-Al_2O_3	17.3	1.9	48.1	5.2	73.2	8.0	138.7	15.1
Fe_2O_3/n-Al_2O_3	35.4	4.3	49.2	6.0	63.3	7.7	147.9	17.9
Fe_2O_3/b-Al_2O_3	31.1	2.4	48.6	3.7	66.0	5.0	145.7	11.1

an undesired result because CH_4 captures hydrogen. On the other hand, on Fe_2O_3 embedded materials, a direct relationship is observed between the pH of the support and the production of H_2 and CH_4 (Fig. 6) in order FA > FN > FB where the materials that were supported in acid alumina are those that have the highest production. The ammonium desorption results of catalysts confirm these activity–acidity dependence, showing more acidity sites assigned to strong acidity in FA material and minor to FN and FB (Table 3). This shows that FA has more acid sites with strong acidity per unit of area than other tested materials, which confirms the effect of alumina pH on HDPE catalysis activity to produce H_2 (Fig. 6). Furthermore, it is possible to observe that the increase in temperature favors the production of H_2 and CH_4 on all the materials.

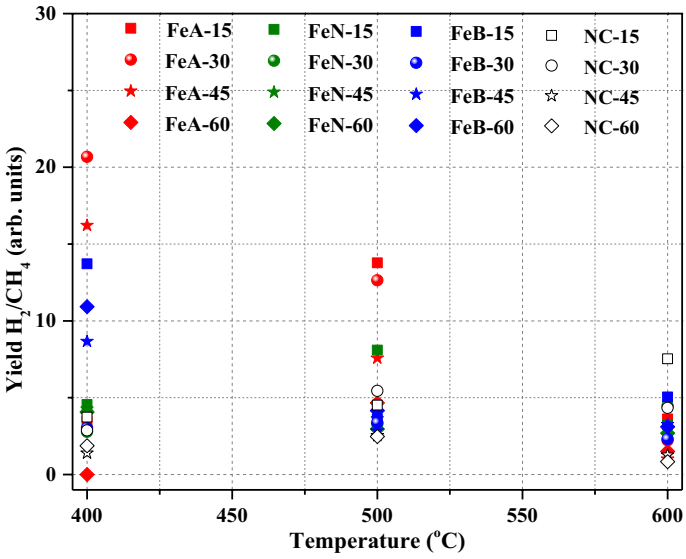

Fig. 7 H_2/CH_4 yield from an HDPE catalytic decomposition at 15 (Square), 30 (Sphere), 45 (Star) and 60 (Diamond) minutes of reaction, with respect to the increase in temperature from 400 to 600 °C (Red: FeA (a-Al_2O_3/Fe_2O_3), green: FeN (n-Al_2O_3/Fe_2O_3), blue: FeB (b-Al_2O_3/Fe_2O_3), black: NC (No catalyst). (Color figure online)

Fig. 7 shows that the H_2/CH_4 ratio changes as a function of temperature, since at 400 °C the production of H_2 is favored and at 600 °C the H_2/CH_4 ratio is very similar. Regarding the pH of the support, it is evident that the materials supported in acidic alumina are more selective to H_2 than n-Al_2O_3 and b-Al_2O_3. Materials showed the following decreasing order FA > FN > FB > NC regarding its H_2 production as a function of their temperature and reaction time. Recalling the relationship discussed above between the production of H_2 and the pH of the supports, these effects are due to the changes on structural properties of the materials, since after increasing the pH of the support the surface area decreases, but the Fe_2O_3 crystal size, particle size and its agglomeration increases (Table 2). All of this explains the decrease in H_2 production. This behavior that has been observed in acidic and basic Al_2O_3 corresponds to that reported by Abid Farooq et al., (2020) where they report that Ni/Al_2O_3 materials present the highest activity for H_2 generation when samples show the highest dispersion of Ni and high surface area [15].

Ni, Fe or Mn-based materials supported on alumina, zeolites and MCM-41 have been reported on reactions like those reported in this work, but using a higher temperature range (between 800 and 850 °C) (Table 4) [20–23]. Those reports show that the Ni-based materials are excellent materials for H_2 production. In comparison to the presented results in this work, some reported materials are apparently better. However, it is important to consider that previous results were obtained at higher temperatures. Enhancing the thermal decomposition of plastics and increasing the total costs of the reaction. FA sample reported in this work shows the greatest H_2 production (47.8 mmol g^{-1} plastic) at only 600 °C, Additionally, the production of H_2 was tested on alumina supports without an active phase, as a result a-Al_2O_3 shows the better yield (2.0 mmol g^{-1} plastic)

Table 4 Comparison of H_2 production, parameters used in the synthesis and the catalytic activity in reported materials and those evaluated in this work

Sample	MET	ST °C	SRT h	C g	CT min	CRT °C	YH_2 $mmol \cdot g^{-1}_{plastic}$	References
Ni/γ-Al_2O_3	I	800	3	0.5	15	800	22.5	[14]
Ni/α-Al_2O_3	I	800	3	0.5	15	800	18.0	[14]
Fe/γ-Al_2O_3	I	800	3	0.5	15	800	22.9	[14]
Fe/α-Al_2O_3	I	800	3	0.5	15	800	20.7	[14]
Ni–Fe/γ-Al_2O_3	I	800	3	0.5	15	800	31.8	[14]
Fe–Ni-MCM-41	I	550	4	0.25	–	800	46.1	[15]
Ni–Mn–Al	C	750	3	0.5	40	800	56.3	[16]
Ni/ZSM5-30	I	500	3	0.5	30	850	66.0	[17]
Ni/β-zeolite-25	I	500	3	0.5	30	850	61.3	[17]
Ni/Y-zeolite-30	I	500	3	0.5	30	850	58.0	[17]
FeA	IWI	600	1	0.2	45	600	47.8	This work
A	IWI	600	1	0.2	60	600	22.0	This work

MET synthesis methodology (*I* impregnation, *C* coprecipitation, *IWI* incipient wet impregnation), *ST* synthesis temperature, *SRT* synthesis reaction time, *C* catalyst, *CT* catalytic reaction time, *CRT* catalytic reaction temperature, YH_2 yield mmol of H_2 generated per g of polymer

(Table 4). Also, Dingding et al., (2018) reported the co-production of H_2 and carbon nanotubes from plastic waste using Ni and Fe-based catalysts supported on alumina at 800 °C. Their results are consistent with those obtained in this work on the FA samples in terms of the generation of carbonaceous solid products and gases, however the H_2 production is higher (FA: 62%) even at lower temperature (600 °C), although the authors use a mixture of polymers, the results obtained from these mixtures are very similar to only using HDPE (case study), this is evident in the work published by Itsaso et al., (2018) where they tested four different plastics: HDPE, PP, PET, PS and their mixture (HDPE, 48 wt%; PP, 35 wt%; PS, 9 wt% and PET, 8 wt%) for the production of H_2, their results showed similar H_2 yields for the mixture of polymers and HDPE [17]. It has been widely reported that catalysts used on this kind of reactions are deactivated due to the surface adsorption of carbonaceous residues, however, catalysts based on transition metal oxides can be re-activated by applying an air flow at the temperature of catalyst preparation [2]. Regarding the stability of the material (Fe_2O_3/a-Al_2O_3) a XRD analysis before and after the hydrogen production reaction was carried out as a result both diffractograms are identical with the only difference that there is a new signal on the after reaction sample at 26.16 degrees of 2 theta that corresponds to crystalline graphitic carbon (01-075-1621 JCPDS) which means that the inactivation mechanism will be the same as has been widely reported but it also states that the material is stable and reusable after the reactivation processes also reported. Due to the obtained and discussed results, we can observe that the synthesis methodology used in this work is simple, fast and appropriate to produce materials with excellent properties to obtain H_2. It is also evident that the materials studied on this work have a better H_2 production (even at low temperatures)

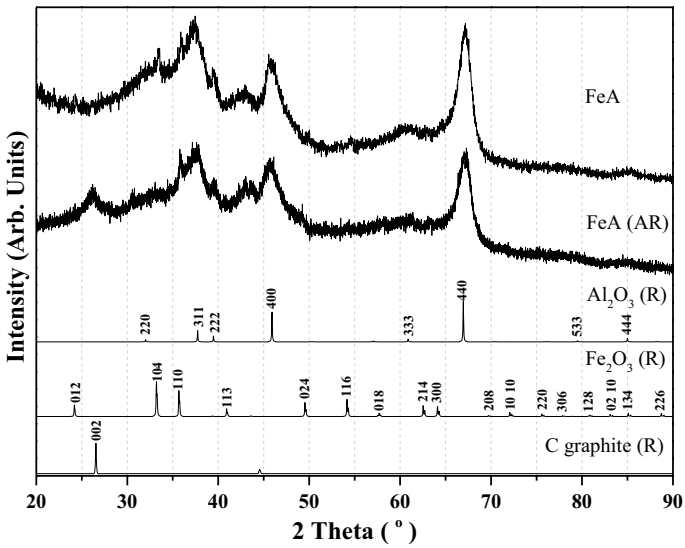

Fig. 8 XRD spectra of catalyst fresh (FeA), after reaction (AR), and reported (R) in data base JCPDS–ICDD

compared to those reported by other authors. As a result, the reported materials are excellent candidates to use in clean fuel processes and H_2 generation (Fig. 8).

Conclusion

In this experimental research work, the effect of the pH of the Al_2O_3 support on the active phase Fe_2O_3 for the production of H_2 from the decomposition of HDPE was confirmed. The Fe_2O_3 supported on acidic Al_2O_3 showed better activity and selectivity (H_2 62%, CH_4 16%) than the Fe_2O_3 supported on alumina at neutral pH and at basic pH, establishing a dependency between the number of strong acid sites on the support and the catalytic activity of Fe_2O_3. Due to the high activity and selectivity of the Fe_2O_3/Al_2O_3 catalytic system at acidic pH, we suggest them as appropriate materials to produce molecular hydrogen.

Acknowledgements The authors acknowledge the funding of this research through grants, PRODEP UABC-PTC-720, UABC-300/6/N/84/19, 300/1/N/175/7, UES-PII-20-UAM-IG-01, and SENER-CONACYT (project 279090). We are very grateful to Gladis J. Labrada D., Araceli Patron S., Beatriz A. Rivera E., Ana I. Peña M., Lucia Aldana N., Miguel Estrada, Lilian B. Romero S., Viridiana Camacho M., and Mariel Quirós C., for technical assistance. We also thank institutions FCQI-UABC, LINAN-IPICYT, and CNYN-UNAM, for providing laboratory support.

Funding The authors acknowledge the funding of this research through the grants, PRODEP UABC-PTC-720, UABC-300/6/N/84/19 and UES-PII-20-UAM-IG-01.

Declarations

Conflict of interest The authors declare no competing financial interest.

References

1. Jubinville D, Esmizadeh E, Saikrishnan S, Tzoganakis C, Mekonnen T (2020) A comprehensive review of global production and recycling methods of polyolefin (PO) based products and their post-recycling applications. Sustain Mater Technol 25:e00188. https://doi.org/10.1016/j.susmat.2020.e00188
2. Palos R, Gutierrez A, Vela FJ, Olazar M, Arandes JM, Bilbao J (2021) Waste refinery: the valorization of waste plastics and end-of-life tires in refinery units. A review. Energy Fuels 35(5):3529–3557. https://doi.org/10.1021/acs.energyfuels.0c03918
3. Rodríguez E, Gutierrez A, Palos R, Vela FJ, Azkoiti MJ, Arandes JM, Bilbao J (2020) Co-cracking of high-density polyethylene (HDPE) and vacuum gasoil (VGO) under refinery conditions. Chem Eng J 382:122602. https://doi.org/10.1016/j.cej.2019.122602
4. Soni VK, Singh G, Vijayan BK, Chopra A, Kapur GS, Ramakumar SSV (2021) Thermochemical recycling of waste plastics by pyrolysis: a review. Energy Fuels 35(16):12763–12808. https://doi.org/10.1021/acs.energyfuels.1c01292
5. Mariappan M, Panithasan MS, Venkadesan G (2021) Pyrolysis plastic oil production and optimisation followed by maximum possible replacement of diesel with bio-oil/methanol blends in a CRDI engine. J Clean Prod 312:127687. https://doi.org/10.1016/j.jclepro.2021.127687
6. Cortazar M, Gao N, Quan C, Suarez MA, Lopez G, Orozco S, Olazar M (2022) Analysis of hydrogen production potential from waste plastics by pyrolysis and in line oxidative steam reforming. Fuel Process Technol 225:107044. https://doi.org/10.1016/j.fuproc.2021.107044

7. Motawie M, Hanafi SA, Elmelawy MS, Ahmed SM, Mansour NA, Darwish MS, Abulyazied DE (2015) Wax co-cracking synergism of high density polyethylene to alternative fuels. Egypt J Pet 24(3):353–361. https://doi.org/10.1016/j.ejpe.2015.07.004
8. Palos R, Gutiérrez A, Vela FJ, Maña JA, Hita I, Asueta A, Bilbao J (2019) Assessing the potential of the recycled plastic slow pyrolysis for the production of streams attractive for refineries. J Anal Appl Pyrol 142:104668. https://doi.org/10.1016/j.jaap.2019.104668
9. Singh N, Hui D, Singh R, Ahuja IPS, Feo L, Fraternali F (2017) Recycling of plastic solid waste: a state of art review and future applications. Composite B 115:409–422. https://doi.org/10.1016/j.compositesb.2016.09.013
10. Ogunola OS, Onada OA, Falaye AE (2018) Mitigation measures to avert the impacts of plastics and microplastics in the marine environment (a review). Environ Sci Pollut Res 25(10):9293–9310. https://doi.org/10.1007/s11356-018-1499-z
11. Ayame A, Uemichi Y, Yoshida T, Kanoh H (1979) Gasification of polyethylene over solid catalysts (Part 3) gasification over calcium X zeolite in a fixed bed tubular flow reactor. J Jpn Petrol Inst 22(5):280–287. https://doi.org/10.1627/jpi1958.22.280
12. Ohkita H, Nishiyama R, Tochihara Y, Mizushima T, Kakuta N, Morioka Y, Tanifuji S (1993) Acid properties of silica-alumina catalysts and catalytic degradation of polyethylene. Ind Eng Chem Res 32(12):3112–3116. https://doi.org/10.1021/ie00024a021
13. Ng SH, Seoud H, Stanciulescu M, Sugimoto Y (1995) Conversion of polyethylene to transportation fuels through pyrolysis and catalytic cracking. Energy Fuels 9(5):735–742. https://doi.org/10.1021/ef00053a002
14. Cai N, Li X, Xia S, Sun L, Hu J, Bartocci P, Chen H (2021) Pyrolysis-catalysis of different waste plastics over Fe/Al_2O_3 catalyst: High-value hydrogen, liquid fuels, carbon nanotubes and possible reaction mechanisms. Energy Convers Manag 229:113794N. https://doi.org/10.1016/j.enconman.2020.113794
15. Farooq A, Song H, Park YK, Rhee GH (2021) Effects of different Al_2O_3 support on HDPE gasification for enhanced hydrogen generation using Ni-based catalysts. Int J Hydrogen Energy 46(34):18085–18092. https://doi.org/10.1016/j.ijhydene.2020.05.199
16. Joint committee on powder diffraction standards international center for diffraction data. 2012.
17. Patterson AL (1939) The Scherrer formula for X-ray particle size determination. Phys Rev 56(10):978. https://doi.org/10.1103/PhysRev.56.978
18. Armenta MA, Maytorena VM, Flores-Sánchez LA, Quintana JM, Valdez R, Olivas A (2020) Dimethyl ether production via methanol dehydration using Fe_3O_4 and CuO over γ–χ–Al_2O_3 nanocatalysts. Fuel 280:118545. https://doi.org/10.1016/j.fuel.2020.118545
19. Kodama H, Schnitzer M (1980) Effect of fulvic acid on the crystallization of aluminum hydroxides. Geoderma 24(3):195–205. https://doi.org/10.1016/0016-7061(80)90023-3
20. Yao D, Zhang Y, Williams PT, Yang H, Chen H (2018) Co-production of hydrogen and carbon nanotubes from real-world waste plastics: Influence of catalyst composition and operational parameters. Appl Catal B 221:584–597. https://doi.org/10.1016/j.apcatb.2017.09.035
21. Zhang Y, Huang J, Williams PT (2017) Fe–Ni–MCM-41 catalysts for hydrogen-rich syngas production from waste plastics by pyrolysis–catalytic steam reforming. Energy Fuels 31(8):8497–8504. https://doi.org/10.1021/acs.energyfuels.7b01368
22. Wu C, Nahil MA, Miskolczi N, Huang J, Williams PT (2014) Processing real-world waste plastics by pyrolysis-reforming for hydrogen and high-value carbon nanotubes. Environ Sci Technol 48(1):819–826. https://doi.org/10.1021/es402488b
23. Yao D, Yang H, Chen H, Williams PT (2018) Investigation of nickel-impregnated zeolite catalysts for hydrogen/syngas production from the catalytic reforming of waste polyethylene. Appl Catal B 227:477–487. https://doi.org/10.1016/j.apcatb.2018.01.050
24. Barbarias I, Lopez G, Artetxe M, Arregi A, Bilbao J, Olazar M (2018) Valorisation of different waste plastics by pyrolysis and in-line catalytic steam reforming for hydrogen production. Energy Convers Manage 156:575–584. https://doi.org/10.1016/j.enconman.2017.11.048